REPORT DOCUMENTATION PAGE

AFRL-SR-AR-TR-03-

0300

Management and Budget, Paperwork Reduction Project (0704-0188), Washington, DC 20503

1. AGENCY USE ONLY (Leave blank)	2. REPORT DATE	3. REPORT TYPE AND DATES COVERED
	29 April, 2003	Final Report: 15 Dec., 2000-15 Dec., 2002

4. TITLE AND SUBTITLE

Full L-S Band Telemetry System

5. FUNDING NUMBERS

G F496200110101

6. AUTHOR(S)

Michael A. Jensen

7. PERFORMING ORGANIZATION NAME(S) AND ADDRESS(ES)

Brigham Young University
A-261 ASB
Provo, UT 84602-1231

8. PERFORMING ORGANIZATION REPORT NUMBER

9. SPONSORING / MONITORING AGENCY NAME(S) AND ADDRESS(ES)

AFOSR
801 North Randolph Street
Room 732
Arlington, VA 22203-1977

10. SPONSORING / MONITORING AGENCY REPORT NUMBER

11. SUPPLEMENTARY NOTES

12a. DISTRIBUTION / AVAILABILITY STATEMENT

A Approved for public release, distribution unlimited

12b. DISTRIBUTION CODE

13. ABSTRACT ***(Maximum 200 Words)***

Recent changes in spectrum availability as well as higher demands for spectrum have motivated the development of telemetry transmit systems capable of fully operating over both L and S telemetry bands. However, enabling operation within these two bands poses new problems in system design. This report presents a prototype system capable of operating between 1.4 and 2.4 GHz, which supports continuous phase modulation (CPM) waveforms such as pulse code modulation (PCM), frequency modulation (FM), and shaped offset quadrature phase shift keying (SOQPSK). The system architecture is detailed, and the prototype performance is discussed. The report also details a transmission scheme that overcomes the detrimental interference created when two antennas are used on an aeronautical telemetry transmitter, a common practice for overcoming signal obstruction that can occur during air vehicle maneuvering. The development leads to symbol error probability expressions that can be applied to assess the performance of the scheme relative to that of traditional schemes. Representative computational examples demonstrate the potential of the method.

20030822 120

14. SUBJECT TERMS	15. NUMBER OF PAGES
Aeronautical telemetry, telemetry transmitter, antenna diversity	17
	16. PRICE CODE

17. SECURITY CLASSIFICATION OF REPORT	18. SECURITY CLASSIFICATION OF THIS PAGE	19. SECURITY CLASSIFICATION OF ABSTRACT	20. LIMITATION OF ABSTRACT
Unclassified	Unclassified	Unclassified	SAR

NSN 7540-01-280-5500

Standard Form 298 (Rev. 2-89)
Prescribed by ANSI Std. Z39-18
298-102

Full L-S Band Telemetry System

Michael A. Jensen
Department of Electrical and Computer Engineering
459 Clyde Building
Brigham Young University
Provo, UT 84602

Abstract

Recent changes in spectrum availability as well as higher demands for spectrum have motivated the development of telemetry transmit systems capable of fully operating over both L and S telemetry bands. However, enabling operation within these two bands poses new problems in system design. This report presents a prototype system capable of operating between 1.4 and 2.4 GHz, which supports continuous phase modulation (CPM) waveforms such as pulse code modulation (PCM), frequency modulation (FM), and shaped offset quadrature phase shift keying (SOQPSK). The system architecture is detailed, and the prototype performance is discussed. The report also details a transmission scheme that overcomes the detrimental interference created when two antennas are used on an aeronautical telemetry transmitter, a common practice for overcoming signal obstruction that can occur during air vehicle maneuvering. The development leads to symbol error probability expressions that can be applied to assess the performance of the scheme relative to that of traditional schemes. Representative computational examples demonstrate the potential of the method.

1. Telemetry Transmitter

One aspect of the standard paradigm for flight test is continuous monitoring of the aircraft via real-time telemetry [1]. Key air vehicle, system functionality, and pilot health information is relayed to facilitate real-time and post-mission analyses. The telemetry is typically accomplished over a radio frequency (RF) link on dedicated portions of the L-Band (1435-1525 MHz) and the upper S-Band (2310-2390 MHz). Air vehicles are assigned specific frequency channels within these bands, with bandwidth allocated according to the unique mission requirements. Existing telemetry transmitters and antennas are restricted to particular bands or, even worse, to discrete frequencies within a given band.

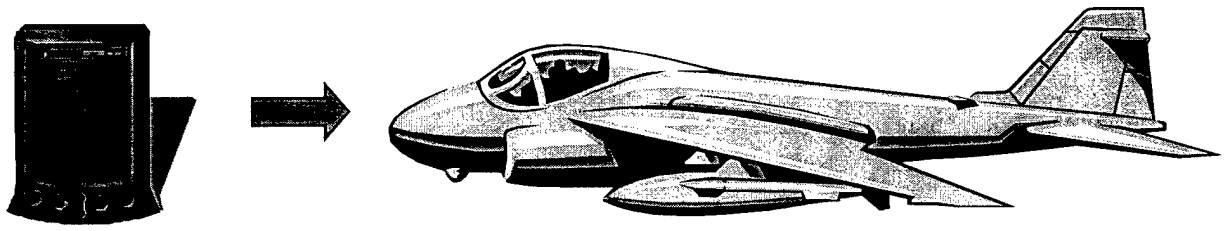

Figure 1: Concept of using a personal digital assistant (PDA) or laptop computer for reconfiguring the frequency channel assignment for an aeronautical telemetry transmitter.

Due to recent changes in spectrum allocation for telemetry and communications, the current hardware infrastructure poses problems in terms of channel assignment and scheduling for air

vehicle telemetry [2]. For example, due to the apparently insatiable demand for RF spectrum in the private sector, portions of the telemetry bands have been reassigned for commercial use. Specifically, congressional actions such as OBRA 93 and BBA 97 have both decreased the bandwidth available for telemetry and fragmented the available channels over the L and S bands. Due to the inflexibility of current hardware, it has become impractical to continue the methods used in the past for channel assignment and scheduling. As a result of this need, new telemetry transmitters must be developed that allow rapid reconfiguration of the transmit band using a laptop computer or personal digital assistant (see Figure 1).

In this report, we discuss the development of a prototype transmitter architecture operating over the L and S bands. The implementation uses commercial off-the-shelf components coupled with custom software. This presentation includes information concerning the system design and performance. We also discuss work that has grown out of this effort that will solve additional problems encountered during air vehicle flight tests.

1.1 Transmitter Architecture

Historical and future trends in aeronautical telemetry suggest that appropriate transmitters be capable of continuous phase modulation (CPM) schemes. Specifically, transmitters should support pulse code modulation (PCM), frequency modulation (FM), and shaped offset quadrature phase shift keying (SOQPSK). Additionally, in order to support operation in both the L and S bands, extreme care must be exercised in generation of the modulated RF signal in order to avoid out-of-band emissions or unwanted in-band signals.

Traditional telemetry transmitters make use of a voltage-controlled oscillator (VCO) whose frequency tuning port is driven both by a center frequency control voltage as well as the modulating baseband data. The architecture used in this prototype is shown in Figure 2. In this design, a programmable phase-lock loop (PLL) subsystem is used in conjunction with a stable 20 MHz reference oscillator in order to accurately control the output frequency of the VCO. The PLL can be controlled directly by the host or through the intermediary of a simple microcontroller. The output power amplifier is typically controlled by the PLL system, being turned on only after the system has acquired lock in order to minimize the transmission of out-of-band signals. The loop filter is designed to remove unwanted signals from the VCO control voltage. Its bandwidth controls the PLL acquisition time and the locked oscillator phase noise performance. In telemetry applications, the system is typically not required to change carrier frequencies during communication. Therefore, the acquisition time is relatively unimportant, and a narrow band loop filter is used in order to optimize the phase noise performance.

The telemetry data are added to the loop filter output voltage in order to modulate the VCO output. The ideal VCO output signal can be expressed as

$$s(t) = A\cos\left[\omega_o t + \phi(t,\alpha) + \phi_o\right] \tag{1.1}$$

where the carrier frequency $\omega_o = K_o V_{PLL}$, K_o is a VCO-dependent constant, and V_{PLL} is the DC voltage at the loop filter output. The data-dependent phase is given as

$$\phi(t,\alpha) = 2\pi h K_o \int_{-\infty}^{t} \sum_{k=-\infty}^{\infty} \alpha_k g(\tau - kT) d\tau \qquad (1.2)$$

where h is a modulation index that depends on the amplitude of the modulating voltage and $g(t)$ is the unity-area single-symbol pulse shape of duration T. For PCM and FM, we use $\alpha_k \in \{-1,+1\}$ with T equal to the symbol period. For SOQPSK, we use $\alpha_k \in \{-1,0,+1\}$ with T equal to one-half of the symbol period and h = ¼ [3]. Therefore, this simple circuit provides the desired CPM waveform provided that the modulating data are properly formatted before its application to the transmitter.

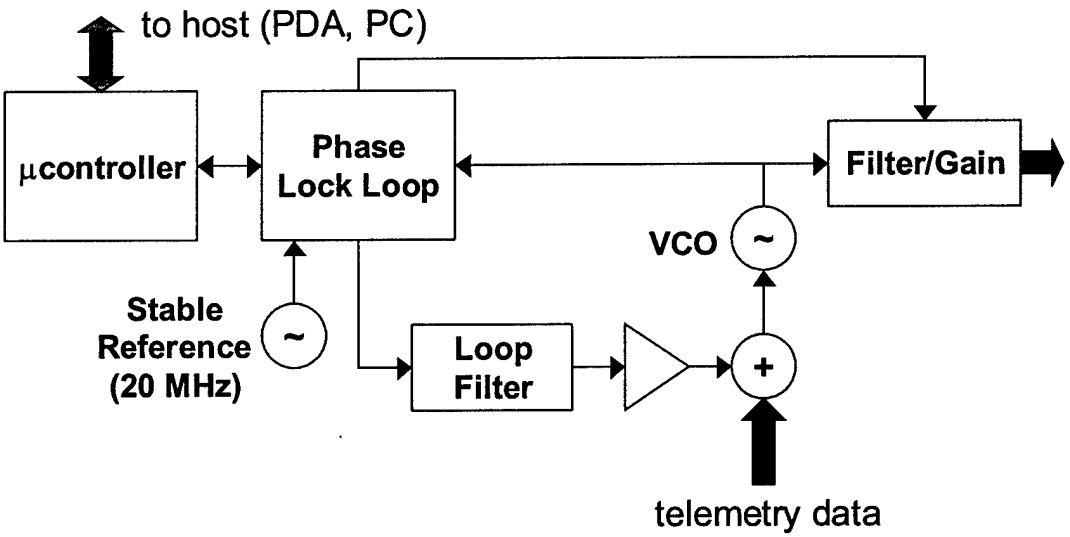

Figure 2: Block diagram illustrating a simple directly modulated voltage controlled oscillator transmitter architecture.

1.1.1 PLL Subsystem

The PLL subsystem consists of the programmable PLL chip, loop filter, 20 MHz reference oscillator, and RF power divider. For this prototype, the LMX2326 PLL chip from National Instruments has been chosen. This chip offers operation between 100 and 2800 MHz with a very high frequency resolution (50 KHz resolution is used for the prototype). Chip programming is accomplished using a serial data interface. The 20 MHz reference signal is an Epson SG-615P crystal oscillator with a frequency stability of $\Delta f / f_o = \pm 100 \times 10^{-6}$.

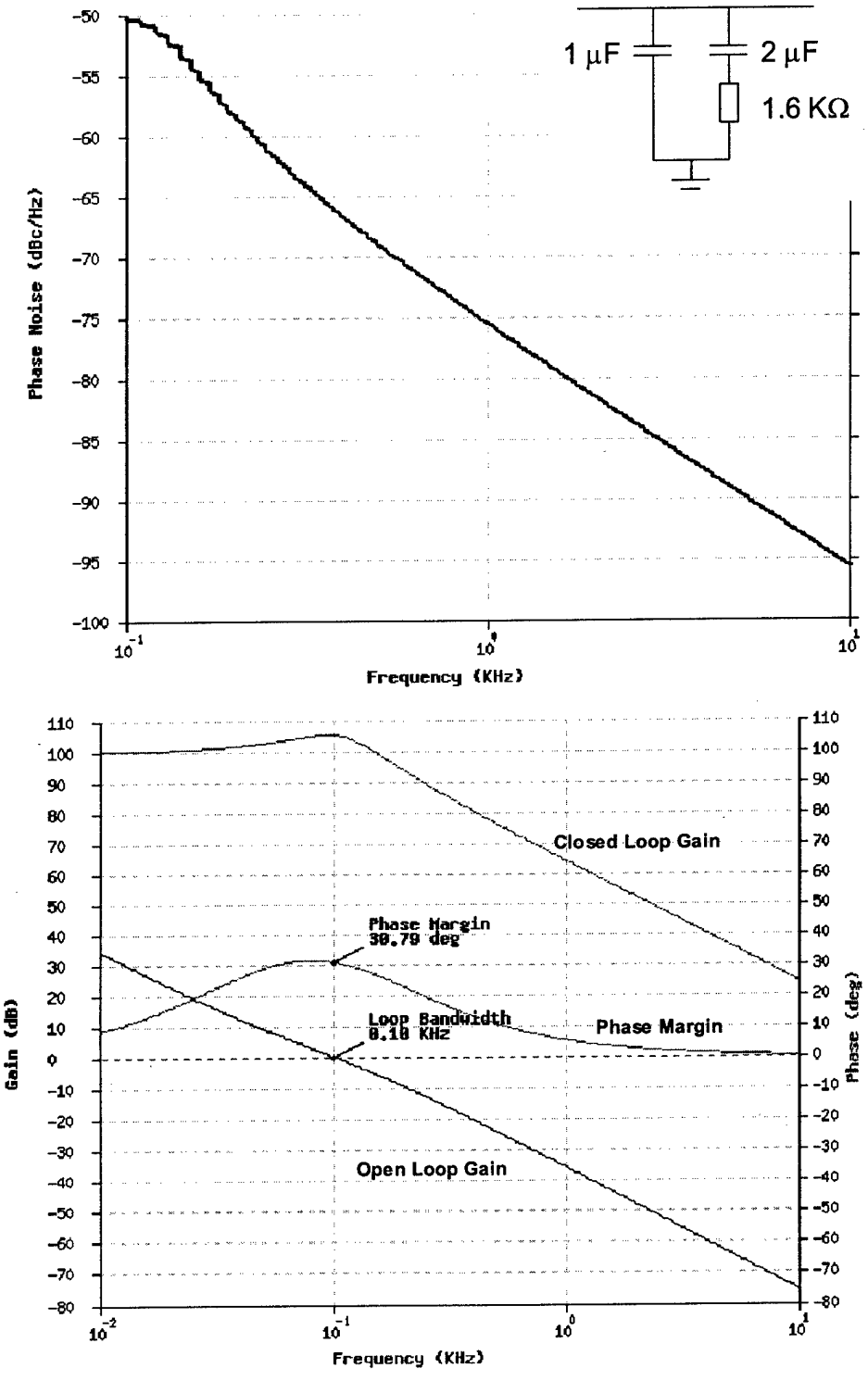

Figure 3: Loop filter design along with predicted phase noise performance and frequency response.

The key design portion of the PLL subsystem involves the loop filter. This filter was designed using standard techniques [4] for a 0.1 KHz loop bandwidth and a 48-degree phase margin. A schematic of the filter, a plot of its frequency response, and a plot of its phase noise performance are shown in Figure 3. As can be seen, the corner frequency is relatively low, which accounts for the excellent phase noise performance. This also results in the relatively long full-scale acquisition time of roughly 70 μS (VCO starts at 1400 MHz and must be locked at 2400 MHz).

The RF power divider is used to split the signal from the VCO between the output port and the RF input to the PLL chip. This has been designed using a simple resistive network such that only -5 dBm of the available 10 dBm output from the VCO is fed back into the PLL chip.

1.1.2 VCO Subsystem

A very wide band VCO is required in order to allow operation over the L and S bands. Fortunately, the ELCO-MS-148/248-01 VCO from Emhiser Research meets the specifications. This surface mount device requires a tuning voltage between 1 and 17 volts for a frequency range of 1430 to 2400 MHz. An op-amp is therefore used to amplify the output of the loop filter to the proper range. The loop filter output is summed with the telemetry data using a simple capacitive/resistive summing circuit. For this prototype, the data signal is generated using a square wave generator, although a more sophisticated system would be utilized in a practical system.

1.1.3 Control Subsystem

A microcontroller is integrated into the programming loop in order to facilitate automatic start-up configuration of the device. The Rabbit 2000 device is chosen, due mainly to the availability of useful and easy-to-use programming tools. A software interface that runs on a personal computer has also been developed to allow simple programming of the device. For the prototype, this software allows full-control of the PLL chipset, although an operational device would implement much of the basic chipset configuration using the automatic start-up sequence at instrument power up. Of most importance is the ability to set the center frequency as well as the device frequency resolution. Figure 4 shows the software interface window.

1.2 System Performance

The entire system was fabricated using surface mount construction on GIL-1000 material (30 mil thickness, 3.26 dielectric constant) and conductor-backed coplanar waveguide technology for the RF interconnects. Once fully integrated, the system achieved a tuning range from 1.14 to 2.48 GHz. The measured phase noise turned out to be approximately –25 dBc at 1 MHz offset, which represents a significant degradation compared to the theoretically computed performance. However, it is known that the spectrum analyzer used to measure this performance suffers from inaccuracies at fine frequency resolution, and therefore further testing is underway to more accurately measure this phase noise performance.

The modulation performance was tested by injecting a square wave (±1) into the telemetry data port. The system output was then down converted using a mixer and a local oscillator (LO). Figure 5 shows the result of this test for a system center frequency of 1400 MHz and LO frequency of 1380 MHz such that the intermediate frequency (IF) is nominally at 20 MHz. The 1 MHz modulating

signal amplitude has been set to exaggerate the frequency modulation behavior. The modulation behavior is clearly very good, although some unwanted amplitude modulation behavior is present. When the modulating waveform was increased in frequency to about 18 MHz, the input capacitance to the VCO began to smooth the transition between the two output frequencies. However, in a realistic system, the telemetry data pulses will undergo shaping in order to limit the transmitted signal bandwidth. As a result, this additional filtering of the data will not significantly degrade the system performance for data rates as high as 20 Mbits per second.

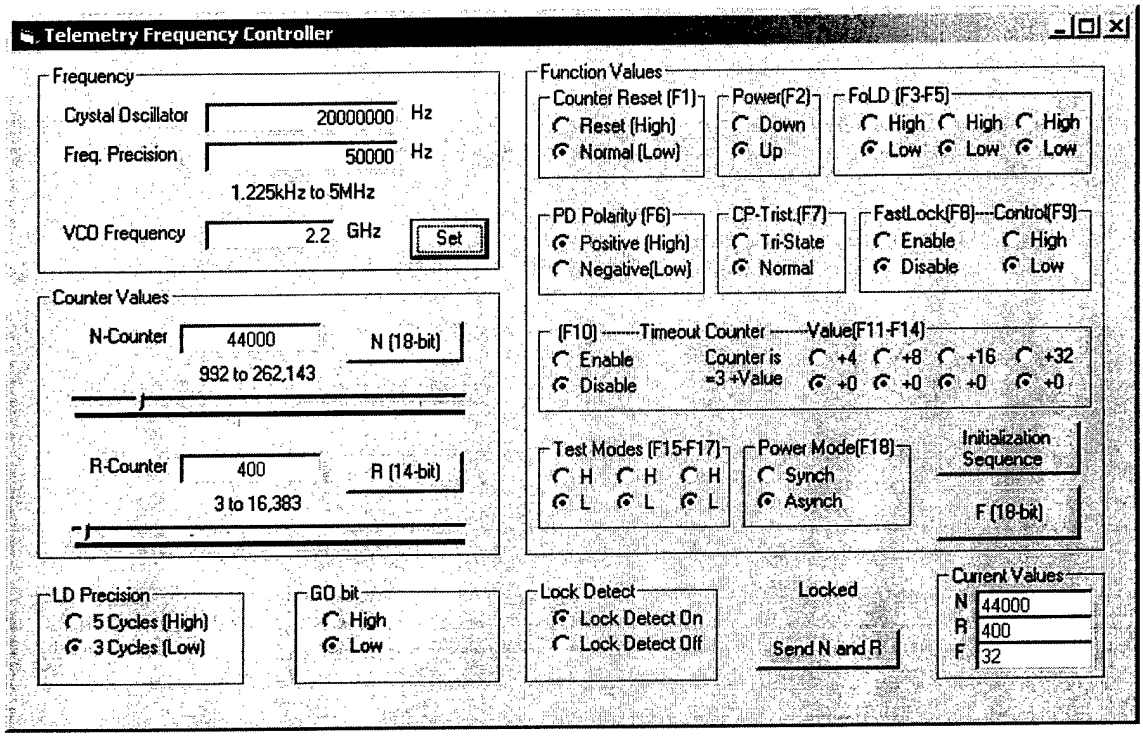

Figure 4: Control window used to program the PLL chip. This interface allows setting the VCO output frequency as well as controlling other features of the device.

1.3 Additional Considerations

1.3.1 Output Filtering and Power Amplification

One of the remaining tasks associated with development of an operational instrument based upon this design involves implementation of output filters and power amplifiers suitable for the bands of interest. Fortunately, new advances in power transistors fabricated using Gallium Arsenide (GaAs) facilitate design of power amplifiers capable of amplifying over the requisite 1 GHz bandwidth. The output filter, on the other hand, will need careful attention in order to adequately suppress out-of-band signals while passing the signals in both operational sub-bands.

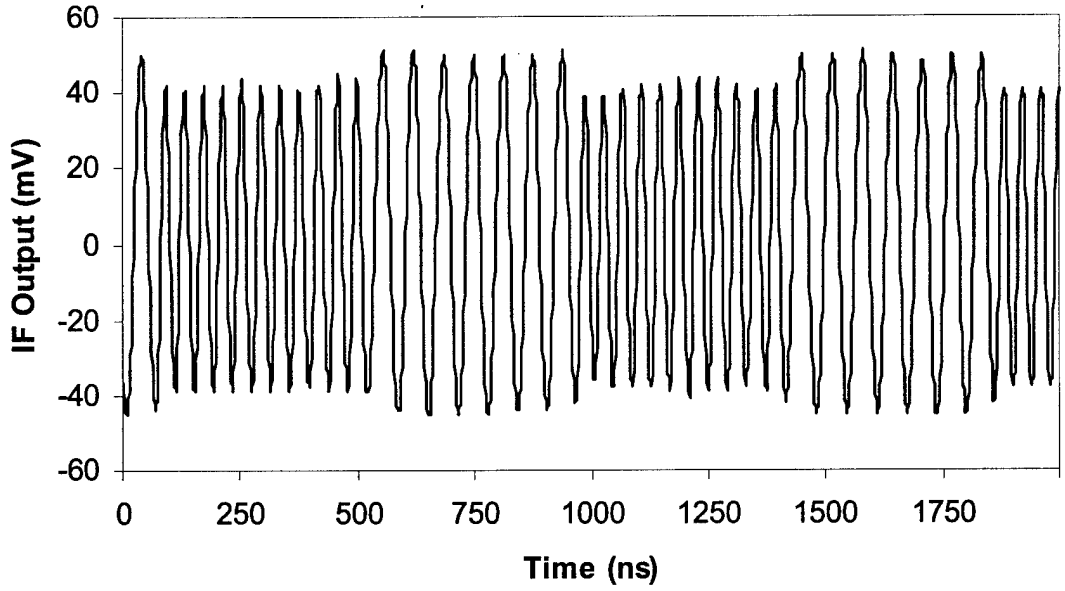

Figure 5: Output waveform resulting from down converting the modulated signal to a 20 MHz intermediate frequency.

1.3.2 Environmental Testing

One of the difficulties with the transmitter architecture examined for this effort is the effect of operational conditions such as temperature or aircraft vibrations. This latter issue is particularly important, since the large tuning range of the VCO can make it highly sensitive to mechanical stresses. As transmitters of this nature are commercialized, extensive environmental testing must be performed in order to determine the system sensitivity to operating conditions. Some of this sensitivity could be reduced by designing a loop filter with a wider loop bandwidth so that the system more quickly adjusts when external influences produce unwanted frequency deviations.

1.3.3 Potential Alternative Architectures

While the merits of the architecture discussed above have been demonstrated by years of use within the telemetry community, the analog introduction of the telemetry data can result in non-ideal output waveform characteristics. To overcome potential limitations of such systems, it is interesting to explore utilization of new technologies that can offer improved performance at reduced costs compared to traditional designs. As an example, consider the architecture shown in Figure 6. This system uses a direct digital synthesizer (DDS), field programmable grate array (FPGA), or digital signal processor (DSP) to directly synthesize the CPM waveform digitally. The In-phase (I) and Quadrature (Q) channels of the synthesized data can then be up converted either by using a programmable source similar to that discussed above or by using a sequence of multiplication stages to create the microwave signal from the IF signal created by the digital subsystem. DDS and FPGA implementations are particularly attractive, since advances in wireless communications system design have resulted in off-the-shelf components capable of producing the desired waveforms at

rates in excess of 100 Mbits/s. Work is currently underway to assess the feasibility and performance advantages and disadvantages associated with using such an architecture.

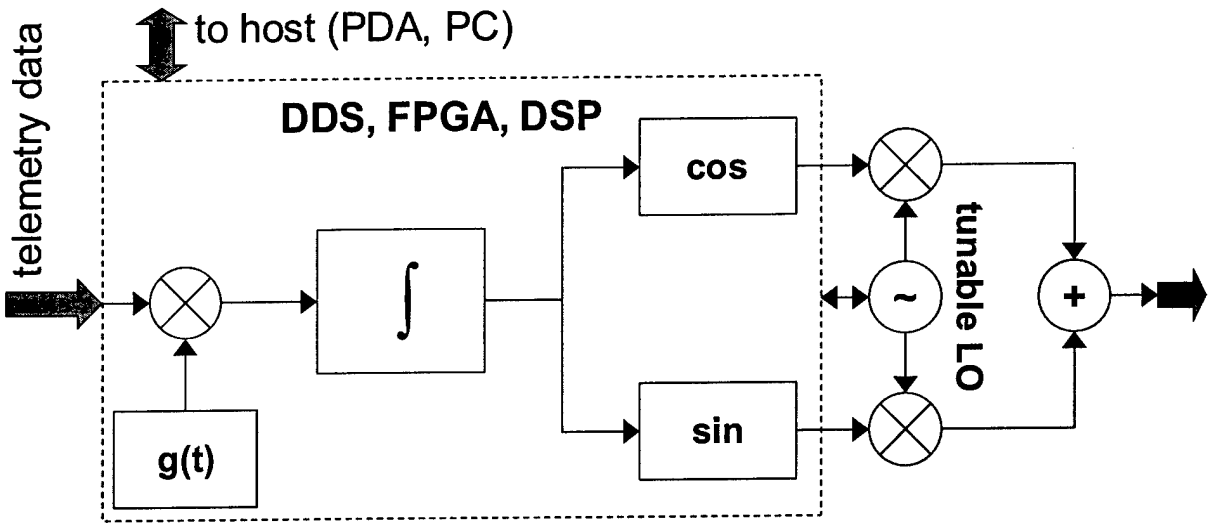

Figure 6: Potential architecture for digital generation of the baseband telemetry transmit stream.

2. Space-Time Coding for Dual-Antenna Telemetry Transmission

The telemetry transmitter detailed above solves one of the problems encountered in aeronautical test and evaluation. Another problem of significant concern is that during aircraft maneuvering, the transmission path for the telemetry data is often obstructed by the aircraft itself. A common solution to this problem is to place a second antenna on the aircraft to ensure the presence of a clear transmission path for all aircraft attitudes. However, when both antennas are in view of the receiver, this arrangement leads to an array interference pattern generally characterized by a large number of transmission nulls. These nulls are clearly detrimental to communication reliability.

The signal variation due to this self-interference is very similar in nature to signal fading created by multipath propagation in wireless communication systems. This observation motivates application of antenna diversity techniques that have been developed for systems operating in multipath environments [5], [6]. One approach that shows particular promise for this application uses a clever transmit diversity scheme in order to reduce detrimental interference [7]. Implementation of the method requires more advanced processing at the receiver, but offers dramatic performance advantages compared to more traditional approaches.

This portion of the report develops this method within the context of dual-antenna aeronautical telemetry links. The formulation leads to expressions for symbol error probability that can be used to assess the performance of the method relative to that of traditional techniques. Representative computational examples demonstrate the dramatic improvement in signal reliability offered by the new method. The section concludes with a brief discussion of outstanding issues that require attention before the scheme can be applied operationally.

2.1 *Dual-Antenna Transmission Schemes*

We begin our study with a careful formulation of the received signals for the traditional and the proposed dual-antenna transmit schemes. Our goal is to obtain a representation that allows analysis of the symbol error rates as well as facilitates a qualitative understanding of the benefit offered by the new approach. In the following, we assume that the antennas 1 and 2 are located at (x_1, y_1, z_1) and (x_2, y_2, z_2) respectively, where the coordinates are expressed in a local coordinate system for the air vehicle. For simplicity of presentation and understanding, we will neglect amplitude and phase variations as a function of angle (i.e. power and phase patterns) for the individual antennas, although it is straightforward to add these variations to the analysis. If the receiving ground station is located at the point (r, θ, ϕ) in spherical coordinates, then the transfer function between the ith antenna, $i \in \{1, 2\}$, and the ground receiver station may be expressed as

$$h_i = e^{jk(x_i \sin\theta\cos\varphi + y_i \sin\theta\sin\varphi + z_i \cos\theta)} \tag{2.1}$$

where $k = 2\pi / \lambda$ is the free-space wavenumber with λ the free-space wavelength.

Consider now transmission using only antenna 1. If the transmitted symbol is denoted as s, the received signal is represented as

$$r_a = h_1 s + \eta \tag{2.2}$$

where η represents the additive white Gaussian noise (AWGN) in the receiver. The received signal energy can be expressed as

$$E_a = \mathrm{E}\{(h_1 s)^* h_1 s\} = \mathrm{E}\{|h_1^2|\}\mathrm{E}\{|s^2|\} = \mathrm{E}\{|s^2|\} = E_s \tag{2.3}$$

where we have used that $|h_1^2| = 1$, $\mathrm{E}\{\cdot\}$ represents an expectation, and E_s is the average symbol energy. The receiver noise power spectral density (PSD) is given as $N_o = \mathrm{E}\{\eta^* \eta\}$, leading to a receive signal-to-noise ratio (SNR) of E_s / N_o. This quantity will be used as a baseline for comparing the performance of the different transmission schemes.

2.1.1 *Traditional Transmission*

For standard two-antenna transmission, each symbol is simultaneously radiated from both antennas. The received signal may be expressed as

$$r = \frac{1}{\sqrt{2}}(h_1 + h_2)s + \eta \tag{2.4}$$

where the factor of $\sqrt{2}$ stems from the fact that the power is equally divided between the two transmit antennas. The received signal energy becomes

$$E_T = \mathrm{E}\left\{\frac{1}{2}\left[(h_1 + h_2)s\right]^*(h_1 + h_2)s\right\} = \frac{1}{2}|h_1 + h_2|^2 \mathrm{E}\left\{s^2\right\} = \frac{1}{2}|h_1 + h_2|^2 E_s \tag{2.5}$$

while the noise PSD is N_o. Therefore, this scheme leads to the received SNR

$$\mathrm{SNR}_T = \frac{1}{2}|h_1 + h_2|^2 \frac{E_s}{N_o}. \tag{2.6}$$

For widely-spaced antennas, which is typical of the situation for dual-antenna telemetry transmitters, the coherent addition of the two transfer functions leads to severe nulls in the gain pattern at certain angles. For example, Figure 7 illustrates a plot of this interference pattern as a function of the angle ϕ for $\theta = 90°$ and the antennas separated by 10λ in the x dimension. Clearly, this gain pattern will cause significant reduction in the communication reliability.

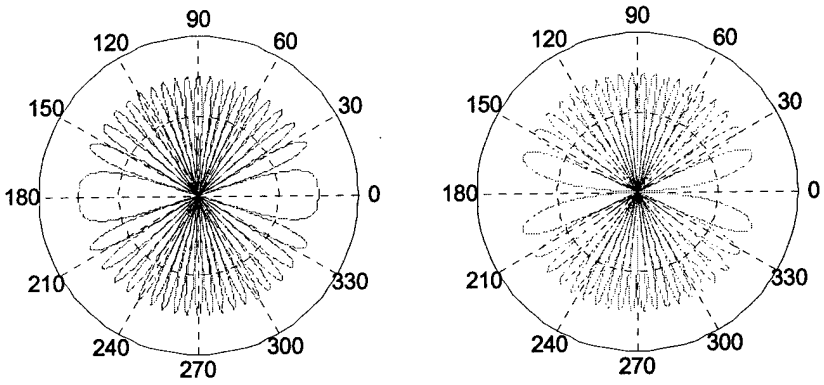

Figure 7: Gain pattern resulting from 2 antennas separated by 10λ for $\theta = 90°$. The two plots are for when the two antennas are in phase and out of phase, respectively.

2.1.2 Diversity Transmission

The transmit diversity scheme proposed here was originally introduced to combat multipath fading for wireless systems. This method, referred to as the Alamouti scheme [7], uses a transmission strategy that spans two consecutive symbol periods. Let the two consecutive symbols be denoted as s_1 and s_2. During the first symbol time, antenna 1 transmits s_1 while antenna 2 simultaneously transmits s_2. During the second time slot, antenna 1 transmits $-s_2^*$ while antenna 2 simultaneously transmits s_1^*. The received signal in the two slots can be expressed as

$$r_1 = \frac{1}{\sqrt{2}}(h_1 s_1 + h_2 s_2) + \eta_1 \tag{2.7}$$

$$r_2 = \frac{1}{\sqrt{2}}\left(h_2 s_1^* - h_1 s_2^*\right) + \eta_2 . \tag{2.8}$$

These equations can be rewritten in the matrix form

$$\mathbf{r} = \begin{bmatrix} r_1 \\ r_2^* \end{bmatrix} = \frac{1}{\sqrt{2}} \begin{bmatrix} h_1 & h_2 \\ h_2^* & -h_1^* \end{bmatrix} \begin{bmatrix} s_1 \\ s_2 \end{bmatrix} + \begin{bmatrix} \eta_1 \\ \eta_2^* \end{bmatrix} = \mathbf{H}\mathbf{s} + \boldsymbol{\eta} . \tag{2.9}$$

Using this form, it is simple to show that symbol detection can be performed using the operation

$$\tilde{\mathbf{r}} = \mathbf{H}^{*T}\mathbf{r} = \frac{1}{2}\left(|h_1|^2 + |h_2|^2\right)\mathbf{s} + \mathbf{H}^{*T}\boldsymbol{\eta} . \tag{2.10}$$

During the first symbol time, the signal energy is

$$E_{A,1} = \mathrm{E}\left\{\left[\frac{1}{2}\left(|h_1|^2 + |h_2|^2\right)\right]^2 s_1^* s_1\right\} = \left[\frac{1}{2}\left(|h_1|^2 + |h_2|^2\right)\right]^2 E_s \tag{2.11}$$

while the received noise PSD is

$$N_{A,1} = \mathrm{E}\left\{\frac{1}{2}\left(h_1^*\eta_1 + h_2\eta_2^*\right)^*\left(h_1^*\eta_1 + h_2\eta_2^*\right)\right\} = \frac{1}{2}|h_1|^2\,\mathrm{E}\left\{|\eta_1|^2\right\} + \frac{1}{2}|h_2|^2\,\mathrm{E}\left\{|\eta_2|^2\right\} = \frac{1}{2}\left(|h_1|^2 + |h_2|^2\right)N_o \tag{2.12}$$

where we have used independence of η_1 and η_2. An identical result is obtained for the second symbol time. The received SNR for this scheme is therefore equal to

$$\mathrm{SNR}_A = \frac{1}{2}\left(|h_1|^2 + |h_2|^2\right)\frac{E_s}{N_o} \tag{2.13}$$

which, for transfer functions of the form of Eq. (2.1) equals the SNR of the single antenna transmission system. Therefore, this Alamouti scheme can completely remove the detrimental effects of the coherent interference created by the introduction of multiple antennas. It is important to point out that this scheme places most of the complexity and computational burden at the receiver. This is appropriate for aeronautical telemetry applications, since it is difficult to add excessive complexity at the transmitter due to constraints on the size of the telemetry transmitter installed on the air vehicle.

At first glance, the performance gain achievable with this simple transmission scheme may seem surprising. Two comments are warranted concerning this result. The first observation to be made is that by altering the symbols transmitted during the second symbol time, the resulting antenna gain pattern will change (due to the change in the relative phasing between the two antenna signals). For example, for Binary Phase Shift Keying (BPSK), if the two consecutive symbols are such that the antenna pattern is that shown in the left of Figure 7 for the first symbol time, then the pattern will be that shown on the right of Figure 7 during the second symbol time. The superposition of these two

patterns leads to a perfectly omnidirectional pattern. Second, it is important to recognize that obtaining these gains requires that the receiver determine the transfer functions h_1 and h_2. This channel estimation adds computational burden to the system, and can introduce errors that will degrade the performance. Efficient mechanisms for estimating the channel for aeronautical telemetry applications are currently under investigation.

2.1.3 Symbol Error Rate

The formulations in the previous section facilitate the development of expressions for the symbol error rate as a function of the single antenna SNR. To see this, consider first that we have a function that represents the probability of a symbol error $P(\varepsilon)$, where ε denotes the symbol error event and the dependence on SNR is implicitly understood. This function is dependent on the modulation constellation used and noise model assumed. For example, for BPSK and Quadrature Phase Shift Keying (QPSK) with AWGN, this function takes the forms [8]

BPSK: $$P_1(\varepsilon) = Q\left(\sqrt{2\frac{E_b}{N_o}}\right) \tag{2.14}$$

QPSK: $$P_2(\varepsilon) = 2Q\left(\sqrt{\frac{E_b}{N_o}}\right) \tag{2.15}$$

$$Q(x) = \frac{1}{2}\operatorname{erfc}\left(x/\sqrt{2}\right) \tag{2.16}$$

where E_b represents the average bit energy.

For the Alamouti scheme, the formulations in the prior section demonstrate that for transfer functions of the form of Eq. (2.1), the probability of symbol error will be identical to that given for the AWGN channel. For the traditional transmission scheme, however, we must modify these expressions. Let $f_\ell(E_b/N_o)$, $\ell \in \{1, 2\}$ represent Eqs. (2.14) and (2.15). Examination of Eq. (2.6) suggests that for the traditional scheme, the conditional symbol error probability functions can be expressed as

$$P_\ell(\varepsilon \mid \theta, \phi) = f_\ell\left(\frac{1}{2}|h_1 + h_2|^2 \frac{E_b}{N_o}\right) \tag{2.17}$$

where the conditional form stems from the dependence of the transfer functions on the angular position of the receiver. If the probability density function (PDF) of these angles for a flight is expressed as $p(\theta, \phi)$, then the average symbol error rate for the flight is given as [8]

$$\widetilde{P}_\ell(\varepsilon) = \int_0^{2\pi}\int_0^{\pi} f_\ell\left(\frac{1}{2}|h_1 + h_2|^2 \frac{E_b}{N_o}\right) p(\theta,\phi)\sin\theta \, d\theta \, d\phi \,. \tag{2.18}$$

For the examples below, we assume that the PDF on the angles is uniformly distributed within the plane of rotation. We should also point out that if the transfer functions do not have unity magnitude

over all angles, then a similar operation must be performed to derive the symbol error probability for the Alamouti scheme.

It is important to recognize that this development extends to all modulation schemes for which an error probability expression is available. Therefore, the general conclusions drawn from the results of this analysis are broadly applicable and not restricted to the two modulation schemes chosen.

2.2 Simulation Results

In order to explore the effectiveness of the Alamouti scheme in removing the detrimental interference effects encountered in dual-antenna telemetry transmission, we evaluate the above expressions for several different scenarios. In all simulations, we assume a horizontal antenna spacing of 20 ft., a vertical separation of 8 ft., a frequency of 1.5 GHz, and a ground antenna 400 ft. in front of the aircraft.

For the various aircraft attitude positions, the position of the ground antenna within the air vehicle coordinate frame is computed using Eulerian angle transformations. For a given aircraft altitude, pitch, and yaw, we spin the aircraft one full rotation in the horizontal plane, calculating the transfer functions h_1 and h_2 at each of 36,000 angular sample points. Numerical evaluation of the integral in Eq. (2.18) is then performed using a simple trapezoidal integration rule. It was necessary to use such fine angular sampling in order to capture the behavior in the deep nulls of the interference pattern.

To begin, we examine the simple case when the aircraft and the receiver are in the same plane. Naturally, this is relatively unrealistic, but serves as a straightforward computational example to demonstrate the performance of the new scheme. Figures 8 and 9 demonstrate the probability of symbol error versus the single-bit SNR for BPSK and QPSK modulations, respectively. As can be seen from these plots, the average symbol error rate performance for the traditional dual-antenna transmission scheme is quite poor. In fact, this behavior is very similar to what is observed for channels experiencing severe multipath fading. On the other hand, application of the Alamouti scheme for transmit diversity provides much better performance, achieving symbol error rates of 10^{-6} for SNR values on the order of 10-15 dB. These results also show that BPSK and QPSK exhibit the same trends, indicating that the method is applicable for a variety of modulation schemes.

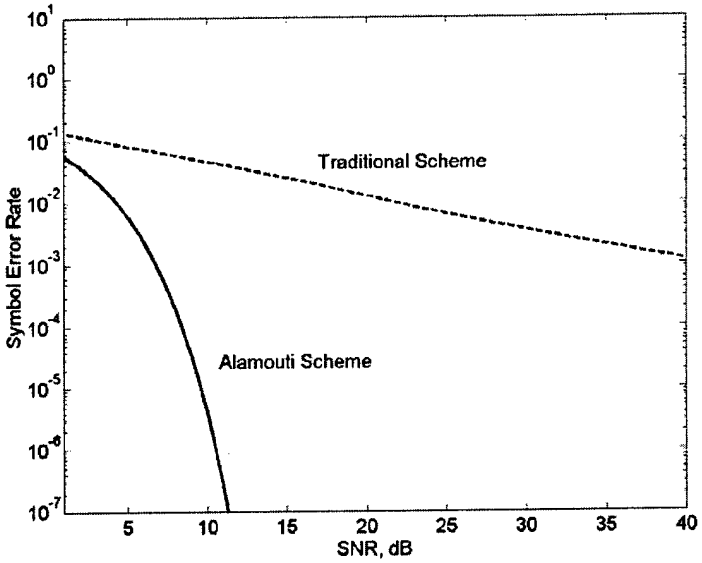

Figure 8: Symbol error rate for Traditional and Alamouti transmission schemes for BPSK modulation with no aircraft elevation.

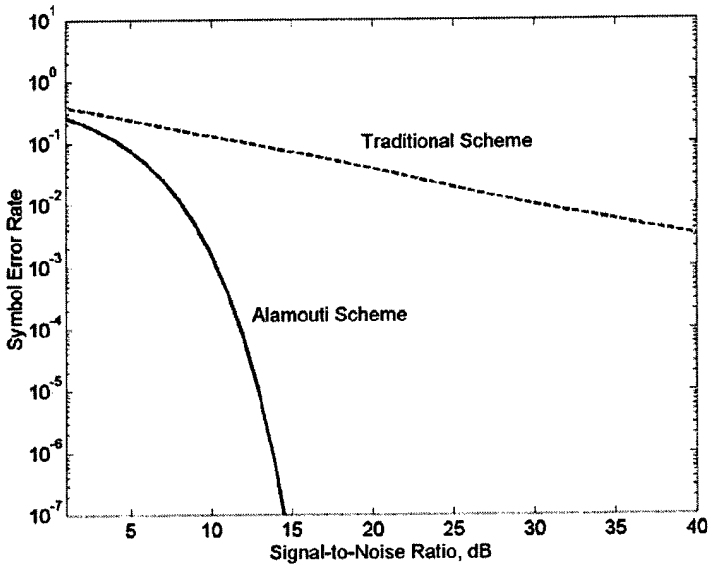

Figure 9: Symbol error rate for Traditional and Alamouti transmission schemes for QPSK modulation with no aircraft elevation.

It is also interesting to examine the behavior of the diversity scheme for a more realistic geometrical configuration. In this case, we assume the aircraft is at an elevation of 2000 ft and at a roll angle of 30° from horizontal. To compute the error probability, the aircraft is then spun in the horizontal plane (relative to the ground coordinate frame). The symbol error probability for this case assuming BPSK modulation is shown in Figure 10. As can be seen, this case exhibits the same behavior as observed in the other examples.

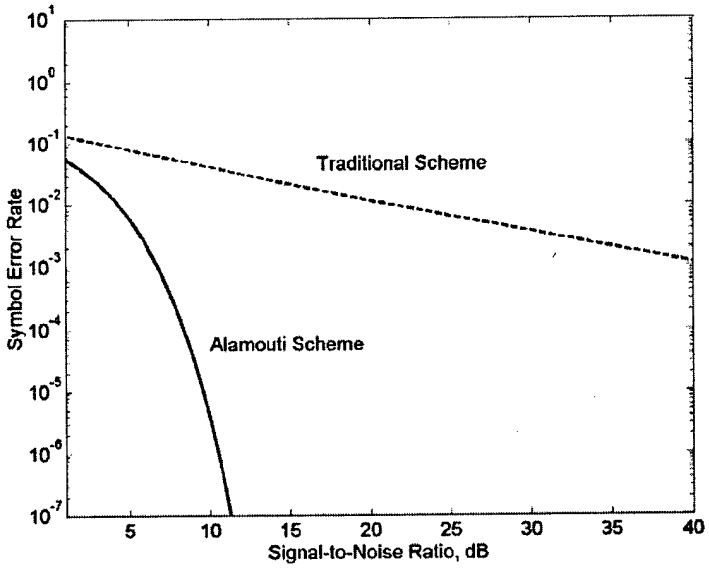

Figure 10: Symbol error rate for Traditional and Alamouti transmission schemes for BPSK modulation with the aircraft at 2000 ft. in elevation and at a 30° roll angle.

2.3 Additional Considerations

While the above developments indicate the potential of the Alamouti transmit diversity scheme for aeronautical telemetry links, there are several issues that must be examined before it can be deployed operationally. These issues will certainly impact the performance of the scheme, and therefore complete evaluation of the method is dependent upon resolution of these issues.

2.3.1 Receive Diversity Implementation

Because air vehicle maneuvering changes the polarization of the transmitted electromagnetic wave, it is important to employ polarization diversity at the receiving station. This implies that the simple transmit diversity scheme must be augmented such that it incorporates two receive channels. This is a relatively straightforward extension of the single receive channel case considered here.

2.3.2 Channel Estimation

Performance of the Alamouti scheme is dependent upon the estimation of the channel transfer functions between the transmit and receive antennas. For an aircraft moving at high velocities, this could be a challenging task since the absolute phase is rapidly varying. However, the task is simplified by the fact that application of the Alamouti scheme depends not on the bulk phase change but rather on the relative phase between the two transfer functions. These phase changes are a result of aircraft attitude variations which occur on a relatively long time scale. Furthermore, if higher order modulation schemes are applied, the receiver will be tracking the bulk phase since this information is necessary for symbol detection.

For high data rates (on the order of 20 Mbits/second), the distance between the two transmit antennas corresponds to a propagation delay that is an appreciable fraction of the symbol period. This means that the two symbols will arrive at the receiver with a significant time offset. Because of this phenomenon, application of the diversity scheme will require compensation for this time shift. This offset will therefore need to be determined during the channel estimation procedure.

3. Conclusions

This report has presented a prototype design for a telemetry transmitter capable of operating in both L and S bands. The system block diagram has been discussed, and the details concerning the implementation have been presented. The performance of the final system was found to meet the specifications for flight test telemetry transmission. Successful implementation of an operational version of this device would significantly increase the flexibility in scheduling frequency channels for aeronautical flight tests.

The report has introduced a new transmit diversity scheme for overcoming detrimental communication conditions created by dual-antenna telemetry transmission. The scheme cleverly alters the symbol transmission such that a two-antenna system can actually achieve the same performance of a single antenna system while overcoming the problem of signal obstruction during air vehicle maneuvering. Symbol error probability expressions have been derived to quantify the relative performance of dual-antenna systems using traditional transmission and the Alamouti scheme. Representative examples demonstrate the dramatic potential impact of this new method.

4. References

[1] Kegel, T., B. Lipe, and J. Swords, "Real-time telemetry data support for the F-22 flight test program," *Proceedings of the 1999 International Telemetering Conference*, pp. 609-619, Las Vegas, NV Oct 25-28, 1999.

[2] Ryan, M. R., "An introduction to spectrum reallocation legislation," *Proceedings of the 1999 International Telemetering Conference*, pp. 399-404, Las Vegas, NV Oct 25-28, 1999.

[3] T. J. Hill, "An enhanced, constant envelope, interoperable shaped offset QPSK (SOQPSK) waveform for improved spectral efficiency," http://www.novaeng.com.

[4] Banerjee, D., *PLL Performance, Simulation, and Design, 2nd Edition*, Dean Banerjee Publishing, 2001.

[5] Foschini, G. J., and Gans, M. J., "On limits of wireless communications in a fading environment when using multiple antennas," *Wireless Personal Communications*, vol. 6, no. 3, pp. 311--335, March 1998.

[6] Raleigh, Gregory G., and Cioffi, John. M., "Spatio-temporal coding for wireless communication," *IEEE Transactions on Communications*, vol. 46, no. 3, pp. 357--366, March 1998.

[7] Alamouti, S. M., "A simple transmit diversity technique for wireless communications," *IEEE J. Selected Areas in Communications*, vol. 16, pp. 1451-1458, Oct. 1998.

[8] Proakis, John G., *Digital Communications*, Fourth Edition, McGraw Hill, Boston, 2001.